

## COMPREHENSIVE STUDY OF NON-UNIFORM CIRCULAR ARRAY INTERFEROMETER IN A REAL TIME BROADBAND 3-DIMENSIONAL DIRECTION FINDER (2–12 GHZ)

M. A. Ebrahimi-Ganjeh\*, M. Soltanian, M. Salarpour, and A. M. Pezeshk

Electronics Research Center, Sharif University of Technology, Tehran, Iran

**Abstract**—A comprehensive study is performed to investigate the performance of a non-uniform circular array interferometer in a real time 3-dimensional direction finder. The angular range of view is supposed to be 65 degrees vertically and 120 degrees horizontally, which is suitable for airborne applications. Interferometer is designed to work in the S, C and X bands. Regarding optimization process, the interferometer employs an eight element non-uniform circular array along with a phase reference antenna at the center of the array. Several quantities and parameters are studied, e.g., frequency behavior, origins of phase measurement errors, Signal to Noise Ratio (SNR) effect on phase measurement, and the effect of the phase measurement error on direction finding performance. The proposed interferometer is able to tolerate at least 35 degrees of phase measurement error. Radius of the array is determined to be 22 cm in order to have good frequency response in the desired frequency band. Both Generalized Regression Neural Network (GRNN) and Maximum Likelihood (ML) estimation are applied for mapping the phase relationships between antennas to the Direction of Arrival (DoA). The results of two methods are well matched, and therefore validation is performed.

### 1. INTRODUCTION

Direction Finding (DF) systems have found important applications in geo-location, navigation, target locating systems, and Electronic Counter Measure (ECM) systems. In comparison with other methods,

---

*Received 12 July 2011, Accepted 30 August 2011, Scheduled 7 September 2011*

\* Corresponding author: Mohammad Ali Ebrahimi-Ganjeh  
(mohammad.ebrahimi@gmail.com).

for higher accuracy and more noise immunity, phase comparison DF system (interferometer) based on the array of antennas is a good choice [1, 2]. The greatest difficulty arising with an interferometer is that for a specific range of view, higher accuracy needs solving more ambiguities [3, 4]. To avoid ambiguity, the phase measurements must be done in an interval with electrical length less than  $2\pi$  or equivalently the employed baseline must be shorter than half of the wavelength [2–4].

In spite of switching beam former with butler matrices [2, 5, 6], Uniform Circular Array (UCA) of antennas has been widely considered for interferometer direction finder [7–10]. In [11], the performance of different direction finding algorithms for the circular arrays is investigated. In general, using a non-uniform array may improve the performance of direction finding [12]. There have been several promising attempts to extend the concept of various direction finding algorithms to arbitrary non-uniform array geometries [13–15]. However, in the most of literature, a comprehensive study, which includes all parts of a practical DF system, frequency behavior, and the effect of systematic errors, is obviously missed.

A new real time 3-D single channel DF system is designed and presented in this paper. The DF algorithm employs neural networks to make the system both real time and more robust to phase measurement errors. Moreover, another method which employs maximum likelihood is applied for validating the results. Phase measurement blocks of the system are explained and origins of phase measurement errors are discussed. The effects of sampling rate and SNR on phase measurement performance are studied. Unlike the most of studies in the literature which consider narrow-band and 2-D direction finding problem, this paper analysis covers 2–12 GHz frequency band as well as the 3-D range of view, which is 65 degrees vertically and 120 degrees horizontally. Even with 35 degrees of phase measurement error, the proposed interferometer is able to achieve the DF accuracy less than 1 degree of RMS in both azimuth and elevation.

## 2. DF ALGORITHMS

### 2.1. Generalized Regression Neural Network and Maximum Likelihood Estimation

The radial-basis function network (RBFN) is a three-layer feedforward network, which is shown in Figure 1. It has universal approximation, optimization, and regularization capabilities. It has been proved that the RBFN can theoretically approximate any continuous function [16]. Radial basis networks may require more neurons than multilayer

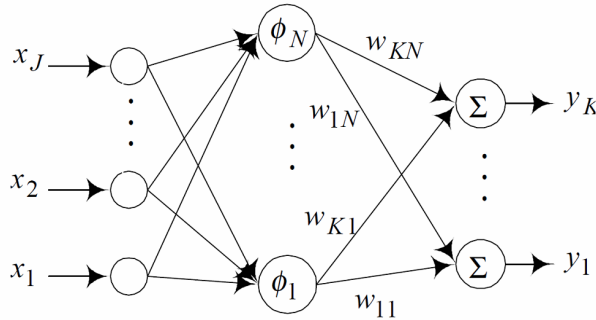


**Figure 1.** Architecture of the RBFN.

perceptron networks, but often they can be designed in a fraction of the time it takes to train standard multilayer networks. They work best when many training vectors are available. One variant of the radial basis network, the Generalized Regression Network (GRNN) consists of radial basis function cells in the first layer [17]. The weights and biases are computed from the input and known output directly.

The phase differences between antennas can be computed from inner product of the DoA vector and the vector of antennas position by Equation (1).

$$\Delta\Psi_{12} = \frac{2\pi}{\lambda} \left( \vec{P}_1 \cdot \hat{a}_n - \vec{P}_2 \cdot \hat{a}_n \right) \quad (1)$$

In Equation (1),  $\lambda$  is the wavelength,  $\vec{P}$  is the vector of antennas position and  $\hat{a}_n$  is the unit vector of DoA. In this paper the generalized regression neural network in each frequency (2 GHz to 12 GHz with step 100 MHz) has been trained with the phase differences between antennas calculated from Equation (1) and DoA in spherical coordinate system varied from  $\varphi = 25^\circ$  to  $\varphi = 156^\circ$  and  $\theta = 85^\circ$  to  $\theta = 161^\circ$  with step  $1.23^\circ$  (coordinate system is shown in Figure 5). To maintain the continuity of the input trained data instead of  $\Delta\Psi_s$  (which jump from  $-\pi$  to  $+\pi$ ) we use sine and cosine of them. The outputs of these networks are azimuth ( $\varphi$ ) and elevation ( $\theta$ ) of DoA. The standard deviation of the radial basis function is determined to be 0.3 after optimization.

Maximum likelihood (ML) techniques were some of the first ones investigated for DoA estimation. Since ML techniques are computationally intensive, they are less popular than other techniques. However, in terms of performance, they are superior to other estimators, especially at low SNR conditions [18]. ML estimation is a procedure that finds the set of parameters which maximize the likelihood function. The likelihood function is the conditional

probability of the observation for measured data sample, assuming the probability density function is predetermined with respect to the parameters [19]. Given a received data sequence  $x(t_n)$ , it is desired to reconstruct the components of the data due only to the desired signals. The parameter values for which the reconstruction approximates the received data with maximal accuracy are taken to be the DoA and desired signal waveform estimates. The approach is to subtract from  $x(t_n)$  an estimate  $A(\hat{\theta}, \hat{\varphi})\hat{s}(t_n)$  of the signal components  $A(\theta, \varphi)s(t_n)$ , where  $x(t_n)$  is the measured data,  $A(\theta, \varphi)$  is the steering matrix of the array and  $s(t_n)$  is the received signal from the array. If the estimates  $(\hat{\theta}, \hat{\varphi})$  and  $\hat{s}(t_n)$  are sufficiently good, the residual  $x(t_n) - A(\hat{\theta}, \hat{\varphi})\hat{s}(t_n)$  will primarily consist of noise and interference with the smallest energy. In other words, minimizing the energy in the residual  $x(t_n) - A(\hat{\theta}, \hat{\varphi})\hat{s}(t_n)$  can result in accurate estimates of  $(\theta_i \approx \hat{\theta}, \varphi_i = \hat{\varphi})$  and  $s(t_n) \approx \hat{s}(t_n)$  with proper choice of  $(\hat{\theta}, \hat{\varphi})$  and  $\hat{s}(t_n)$ . The method can be stated mathematically in a least-squares form as

$$\min_{\theta, \varphi, \hat{s}(t_n)} \left\langle \left\| x(t_n) - A(\hat{\theta}, \hat{\varphi})\hat{s}(t_n) \right\|^2 \right\rangle_N \quad (2)$$

for which the best least squares fit between the received signal and a reconstruction of the signal components is sought [19].

In this paper, the measured data ( $x(t_n)$ ) is the measured phase difference of each antenna with respect to the reference antenna. The steering matrix ( $A(\theta, \varphi)$ ) is computed with step equal to 0.1 degree in both azimuth ( $\varphi$ ) and elevation ( $\theta$ ) according to Equation (1) and the received signal ( $s(t_n)$ ) is assumed to be equal to unity.

## 2.2. Phase Measurement System and Phase Measurement Error

If the product of  $\cos(\omega t + \Psi_1)$  and  $\cos(\omega t + \Psi_2)$  passes through an appropriate flat low pass filter (LPF), the output would be  $\cos(\Delta\Psi_{12})$ . However, If the product of  $\sin(\omega t + \Psi_1)$  and  $\cos(\omega t + \Psi_2)$  does the same, the output would be  $\sin(\Delta\Psi_{12})$ . This is the main idea of using 90 degrees hybrid coupler in the path of reference signal to detect the phase differences between the signals of other antennas and the reference one.

Phase measurement system based on hybrid coupler is depicted in Figure 2. Simulation result with Advanced Designed System (ADS), for inverse tangent of the ratio  $\frac{V_{out\_sin}}{V_{out\_cos}}$  is shown in Figure 3. In this simulation, the signal power values at the output of the antennas are  $-64$  dBm, the phase difference between the signals is 70 degrees, and

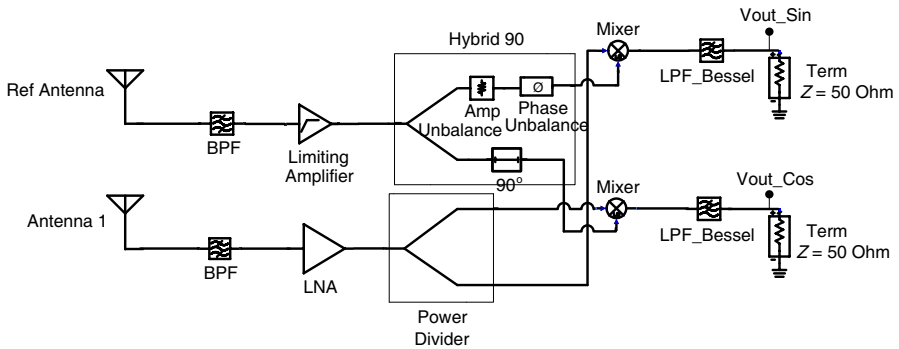


**Figure 2.** Phase measurement system with Hybrid coupler. The output of limiting amplifier is approximately 0 dBm and the gain of LNA is 30 dB.

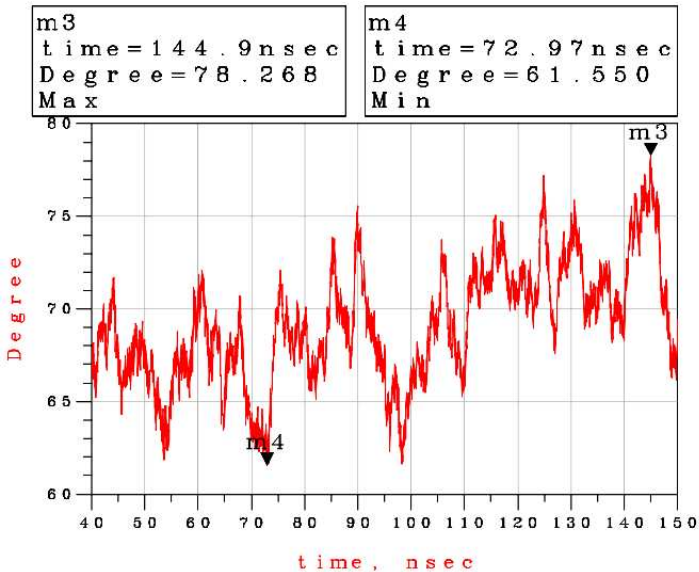


**Figure 3.** ADS simulation result for the system shown in Figure 2. Signal power is  $-64$  dBm at the output of the antenna and the phase difference between the signals is 70 degrees. Minimum and maximum of the phase difference estimation are m4 and m3 respectively.

maximum available noise has been considered. Moreover, amplitude unbalance of the hybrid coupler is considered to be 2 dB and phase unbalance is zero.

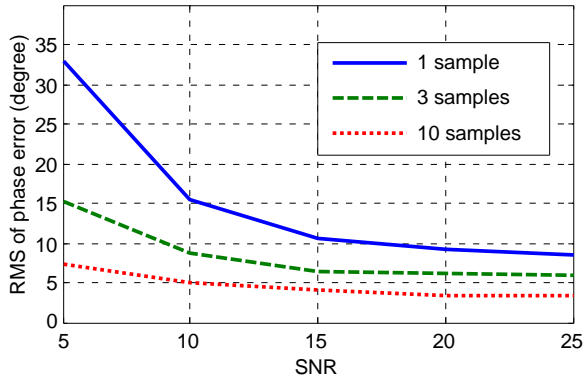


**Figure 4.** Noise and sampling effect on phase measurement error.

In practice, phase unbalance of the  $90^\circ$  hybrid coupler (and maybe some power dividers and mixers) in the wideband application is not negligible. Typical  $90^\circ$  hybrid couplers in the band 2 GHz to 12 GHz have 5 degrees phase unbalance. However, with some calibration process in digital signal processing (in the various frequencies) these errors can be reduced to zero. Moreover, wideband antennas like spiral typically have 5 degrees phase tracking error in their range of view which should be added to the phase measurement error.

Now, assume that all the elements and antennas in the phase measurement system are ideal and without phase and amplitude mismatch. Therefore, the presence of noise in the phase measurement channels is the only source of phase error. Figure 4 shows the root mean square error of phase measurement for various SNR (random Gaussian noise has been considered) in the output of the low pass filter (LPF) in Figure 2. Moreover, Figure 4 shows that by averaging more samples the phase error due to the noise can be reduced.

### 2.3. Interferometer Modules and Optimized Circular Array Structure

Several simulations have been performed to have the best unambiguous response in the band 2–12 GHz. A configuration which resolves ambiguities satisfactorily at the highest frequency will do at least as well at any lower frequency, and in general, accuracy will decrease with decreasing frequency [3]. Figure 5 shows both the elements position in the optimized circular array and the coordinate system which is used in all results of this paper. The radius of the circular array is 22 cm. This array is optimized to have good response in the 65 degrees

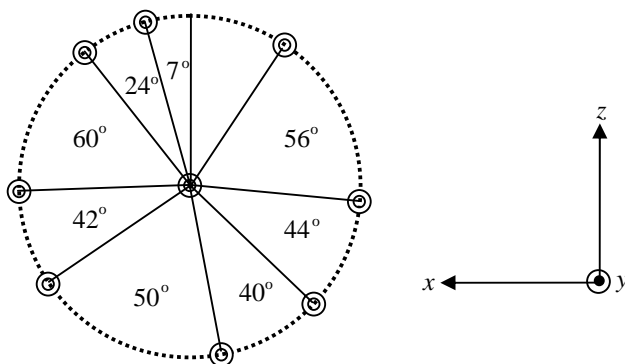


**Figure 5.** Proposed circular array and the coordinate system of this research.

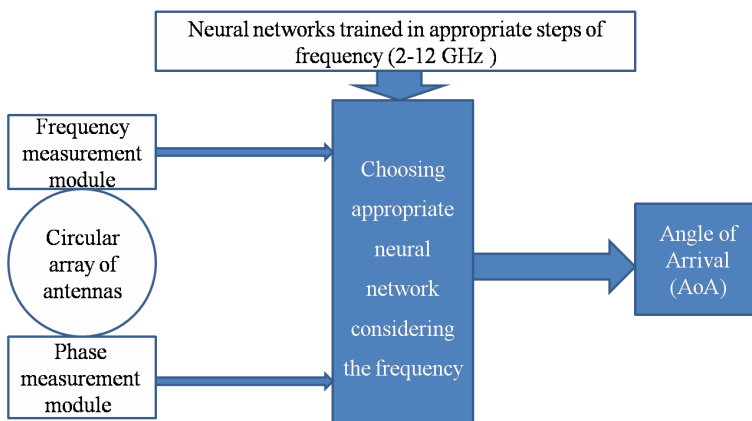


**Figure 6.** General block diagram of the proposed interferometer.

elevation range ( $90^\circ < \theta < 155^\circ$ ) and 120 degrees azimuth range ( $30^\circ < \varphi < 150^\circ$ ).

Figure 6 shows the general block diagram of the interferometer. Instantaneous frequency measurement (IFM) receiver determines the frequency of the incident pulse. The phase measurement system simultaneously finds the phase differences among the signals of the antennas. Because of the low speed of ML method, and to make the interferometer real time, the main DF algorithm of the interferometer employs the generalized regression neural network for hardware implementation [16]. After the phase and frequency measurement, the appropriate neural network, which is trained in the nearest frequency

to the received signal frequency, is chosen to map the phase relations between antennas to the DoA.

### 3. RESULTS

Tables 1 and 2 compare the results of the DF algorithms based on neural network and maximum likelihood in various frequencies. The maximum phase measurement error is considered to be 35 degrees which has Gaussian power spectral density. In this comparison, just two DoA values in 3-D coordinate system ( $[\theta = 100^\circ, \varphi = 45^\circ]$  and  $[\theta = 150^\circ, \varphi = 135^\circ]$ ) have been examined (considering the low speed of ML method which is at least 100 times slower than neural network method in the simulation). Tables 1 and 2 show that the accuracy of GRNN method is really acceptable compared with ML method. Therefore, in the other simulations for the interferometer, we focus just on GRNN method for DF algorithm.

**Table 1.** NN method in compared with ML method for  $\theta = 100^\circ$ ,  $\varphi = 45^\circ$ .

Freq. (GHz)	ML method		NN method	
	$\theta$	$\varphi$	$\theta$	$\varphi$
2	100.7	44.7	100.2	44.5
4	99.1	46.6	100	45
6	100	44.8	99.8	44.9
8	100.3	44.8	99.8	44.7
10	100.1	45.1	99.8	44.7
12	99.9	45	99.8	44.7

**Table 2.** NN method in compared with ML method for  $\theta = 150^\circ$ ,  $\varphi = 135^\circ$ .

Freq. (GHz)	ML method		NN method	
	$\theta$	$\varphi$	$\theta$	$\varphi$
2	148.2	131	149.7	135.2
4	150.2	132.7	149.9	135.1
6	149.5	134.8	150.1	134.4
8	150.1	136.3	150.2	134.8
10	150	135.1	150.2	134.7
12	150.3	135.4	150.2	135.5

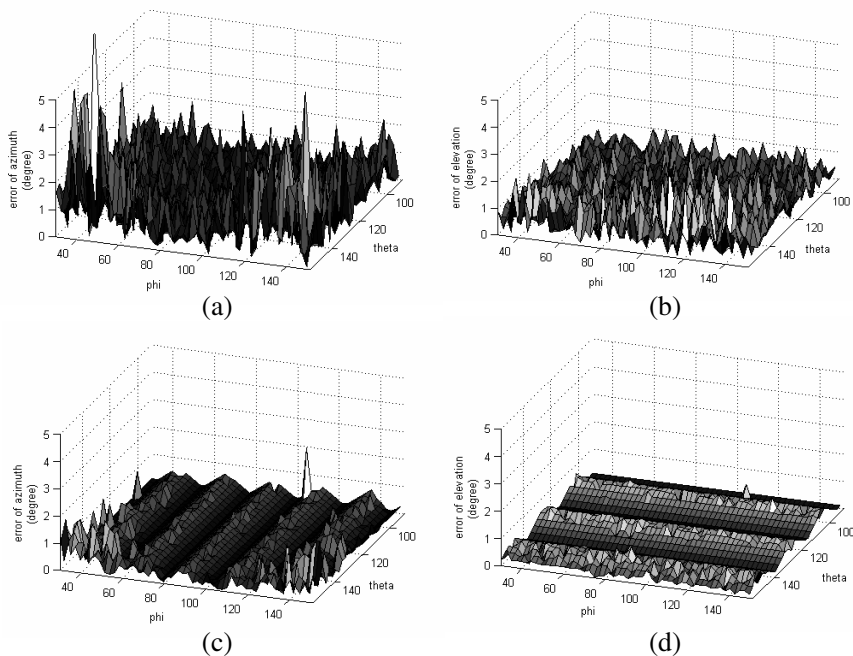


**Figure 7.** 3-D error for azimuth ( $\varphi$ ) and elevation ( $\theta$ ) angle of arrival. (a) and (b) are the azimuth and elevation errors of DoA in 2 GHz. (c) and (d) are the same errors in 12 GHz. The maximum phase measurement error is 35 degrees.

Figure 7 depicts 3-D plot of error for azimuth ( $\varphi$ ) and elevation ( $\theta$ ) estimation of DoA, with step 2.3333 degrees, in upper (12 GHz) and lower (2 GHz) frequencies. Phase measurement error is supposed to be 35 degrees. As Figure 7 shows, it is predictable that in lower elevations (larger values of  $\theta$ ) more estimation error appears. Moreover, in the upper and lower azimuth values the accuracy of azimuth estimation decreases. Another result of these figures is that in higher frequencies, the accuracy of DoA estimation is better than lower frequencies.

Figure 8 shows the RMS error of azimuth and elevation in the frequency band of 2 to 12 GHz with step 50 MHz in the presence of 35 degrees of phase measurement error. It should be mentioned that neural networks are trained every 100 MHz in the frequency interval. Therefore, the error increasing in each 50 MHz is due to the frequency interpolation. For example, in 2250 MHz the algorithm uses the GRNN network trained in 2300 MHz. Therefore, the error increases due to the

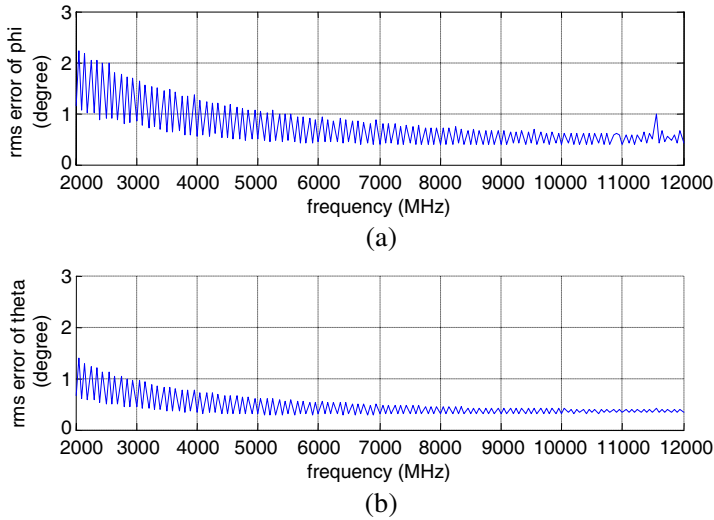


**Figure 8.** RMS error of (a) azimuth and (b) elevation in the frequency band 2 to 12 GHz with step 50 MHz. Neural networks have been trained with step 100 MHz. The maximum phase measurement error is considered to be 35 degrees.

frequency mismatch between the incident signal and the trained neural network. In the frequencies below 6 GHz this interpolation effect can degrade the performance of the system up to 1 degree of RMS. By decreasing the step of network training for the frequencies below 6 GHz, this effect can be mitigated to some extent. For example, if the step is reduced from 100 MHz to 50 MHz, the performance degradation due to the interpolation effect would decrease to less than 0.5 degree of RMS as it can be seen in the frequencies above 6 GHz.

Now, let consider a harsher situation and suppose that the maximum phase measurement error can reach to 47 degrees. Figure 9 shows the RMS error of azimuth and elevation in the frequency band of 2 to 12 GHz with the step 50 MHz for the new condition. The algorithm is still robust to this harsh situation. However, in higher frequencies especially for azimuth DoA estimation some ambiguities happens in the algorithm response which degrades the performance of the system more than 1 degree of RMS. It should be noted that phase measurement errors more than 47 degrees are rare in practical phase measurement systems.

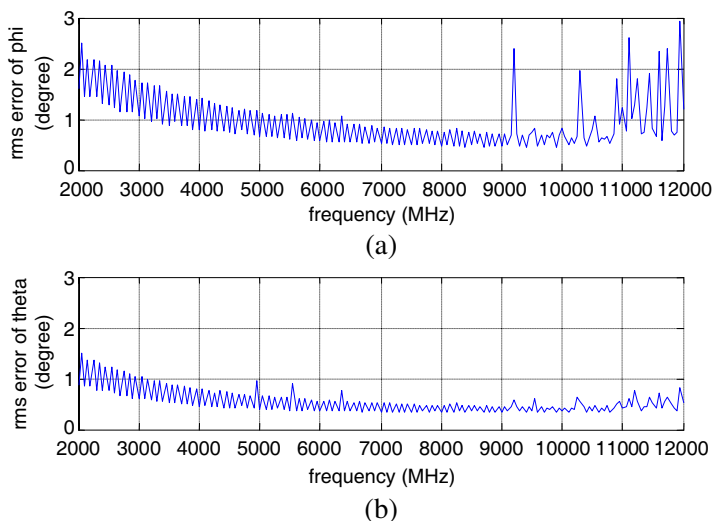


**Figure 9.** RMS error of (a) azimuth and (b) elevation in the frequency band 2 to 12 GHz with step 50 MHz. Neural networks have been trained with step 100 MHz. The maximum phase measurement error is considered to be 47 degrees.

#### 4. CONCLUSION

A comprehensive study was performed to investigate the performance of wideband non-uniform circular array interferometer in a real time 3-D direction finder. A generalized regression neural network was chosen to map the phase relationships between antennas to DoA. Validation was performed by comparing the results of GRNN method with ML one. The phase measurement system was discussed and simulated and the phase measurement error was studied. It was shown that with using more samples, the effect of Gaussian noise on phase measurement error decreased. Then, the effect of phase measurement error on estimating the DoA was investigated and the performance of new interferometer was examined. By using both non-uniform circular array and the DF algorithm based on neural network, a very robust interferometer to phase measurement errors was presented. The proposed interferometer could easily tolerate phase measurement errors for even more than 35 degrees. Also, Frequency behavior of the system was examined and it was shown that the frequency response of the system was acceptable in the whole frequency band.

## REFERENCES

1. *Electronic Warfare and Radar Systems Engineering Handbook*, revision 2, Naval Air Systems Command and Naval Air Warfare Center, Washington, D.C. 20361, 1999.
2. Wiley, R. G., *ELINT: The Interception and Analysis of Radar Signals*, Artech House, 2006.
3. Jacobs, E. and E. W. Ralston, "Ambiguity resolution in interferometry," *IEEE Trans. on Aerospace and Electronic Systems*, Vol. 17, No. 6, 766–780, 1981.
4. Lipsky, S., *Microwave Passive Direction Finding*, SciTech, 2004.
5. Suarez-Fajardo, C., M. Ferrando-Batallur, A. Valero-Nogueira, and V. Rodrigo, "Multiple beam system with circular arrays," *Antennas and Propagation Society International Symposium*, Vol. 4B, 35–38, 2005.
6. Suarez-Fajardo, C., M. Ferrando-Bataller, and A. Valero-Nogueira, "Pattern synthesis of uniform circular arrays with directive elements," *Antennas and Propagation Society International Symposium*, Vol. 3, 2812–2815, 2004.
7. Xun, Y. and Z.-Z. Cui, "Two-dimensional circular array real-time phase interferometer algorithm and its correction," *2nd International Congress Image and Signal Processing*, 1–5, 2009.
8. Mathews, C. P. and M. D. Zoltowski, "Eigenstructure techniques for 2-D angle estimation with uniform circular arrays," *IEEE Transactions on Signal Processing*, Vol. 42, 2395–2407, 1994.
9. Ramos, J., C. P. Mathews, and M. D. Zoltowski, "FCA-ESPRIT: A closed-form 2-D angle estimation algorithm for filled circular arrays with arbitrary sampling lattices," *IEEE Transactions on Signal Processing*, Vol. 47, No. 1, 213–217, Jan. 1999.
10. Zhang, X., Y. Shi, and D. Xu, "Novel blind joint direction of arrival and polarization estimation for polarization-sensitive uniform circular array," *Progress In Electromagnetics Research*, Vol. 86, 19–37, 2008.
11. Tan, C., P. Fletcher, M. Beach, A. Nix, M. Landmann, and R. Thoma, "On the application of circular arrays in direction finding. Part I: Investigation into the estimation algorithms," *IEEE 1st Workshop on Opportunities of the Multidimensional Propagation Channel*, 29–30, 2002.
12. El-Kassis, C., J. Picheral, and C. Mokbel, "EM-ESPRIT algorithm for direction finding with nonuniform arrays," *IEEE 14th Workshop on Statistical Signal Processing*, 453–457, 2007.

13. Rubsamen, M. and A. B. Gershman, "Direction-of-arrival estimation for nonuniform sensor arrays: From manifold separation to fourier domain MUSIC methods," *IEEE Transactions on Signal Processing*, Vol. 57, No. 2, 588–599, 2009.
14. Yasar, T. K. and T. E. Tuncer, "Wideband DOA estimation for nonuniform linear arrays with Wiener array interpolation," *IEEE 5th Workshop on Sensor Array and Multichannel Signal Processing Workshop*, 207–211, 2008.
15. Rubsamen, M. and A. B. Gershman, "Root-music based direction-of-arrival estimation methods for arbitrary non-uniform arrays," *IEEE International Conference on Acoustics, Speech and Signal Processing*, 2317–2320, 2008.
16. Du, K. L., A. K. Y. Lai, K. K. M. Cheng, and M. N. S. Swamy, "Neural methods for antenna array signal processing: A review," *Elsevier Science Signal Processing*, Vol. 82, No. 4, 547–561, 2002.
17. Demuth, H. and M. Beale, *Neural Network Toolbox User's Guide*, Version 4, MathWorks Inc., 2002.
18. Chen, Z., G. Gokeda, and Y. Yu, *Introduction to Direction-of-arrival Estimation*, Artech House, 2010.
19. Chandran, S., *Advances in Direction-of-arrival Estimation*, Artech House, 2005.